

On the quantum stability of Q-balls

Anders Tranberg,^a David J. Weir^b

^a*Faculty of Science and Technology, University of Stavanger, 4036 Stavanger, Norway*

^b*Department of Physics and Helsinki Institute of Physics, PL 64 (Gustaf Hällströmin katu 2), FI-00014 University of Helsinki, Finland*

ABSTRACT: We consider the evolution and decay of Q-balls under the influence of quantum fluctuations. We argue that the most important effect resulting from these fluctuations is the modification of the effective potential in which the Q-ball evolves. This is in addition to spontaneous decay into elementary particle excitations and fission into smaller Q-balls previously considered in the literature, which – like most tunnelling processes – are likely to be strongly suppressed. We illustrate the effect of quantum fluctuations in a particular model ϕ^6 potential, for which we implement the inhomogeneous Hartree approximation to quantum dynamics and solve for the evolution of Q-balls in 3+1 dimensions. We find that the stability range as a function of (field space) angular velocity ω is modified significantly compared to the classical case, so that small- ω Q-balls are less stable than in the classical limit, and large- ω Q-balls are more stable. This can be understood qualitatively in a simple way.

KEYWORDS: Solitons Monopoles and Instantons, Lattice Quantum Field Theory

Contents

1	Introduction	1
1.1	Quantum decay: prelude	3
1.2	Quantum decay: homogeneous Hartree approximation	4
1.3	This paper	5
2	The inhomogeneous Hartree approximation	6
2.1	Ensemble bosons	8
2.2	Global and local observables	9
2.3	Renormalisation	10
3	Results	11
4	Conclusion	14

1 Introduction

Q-balls are a type of localised, periodic solution to certain non-linear field theories, with a net electric charge [1]. They are a form of nontopological soliton [2]. When they exist, Q-balls are classically stable under small perturbations of their shape and radial field profile. In particular, they are spherically symmetric, and the profile can generically be written as (for a complex scalar field ϕ)

$$\phi(t, r) = \frac{\sigma_\omega(r)}{\sqrt{2}} e^{i\omega t}, \quad (1.1)$$

with $\sigma_\omega(r)$ some ω -dependent, but constant in time, profile function. Then the charge is

$$Q = \int d^3x i \left[(\partial_t \phi)^\dagger \phi - \phi^\dagger (\partial_t \phi) \right] = 8\pi\omega \int r^2 \sigma_\omega^2(r) dr. \quad (1.2)$$

The profile function $\sigma_\omega(r)$ can be found by numerically solving the spatial “equation of motion”

$$\left[\partial_r^2 + \frac{2}{r} \partial_r \right] \sigma_\omega(r) = \frac{dV_\omega(\sigma)}{d\sigma}, \quad (1.3)$$

where

$$V_\omega(\sigma) = V(\sigma) - \frac{\omega}{2} \sigma^2(r), \quad (1.4)$$

and $V(\sigma)$ is the classical potential. This simply follows from inserting the ansatz, Eq. (1.1), into the action

$$S = - \int d^3x dt \left[(\partial_\mu \phi)^\dagger (\partial^\mu \phi) - V(\phi) \right]. \quad (1.5)$$

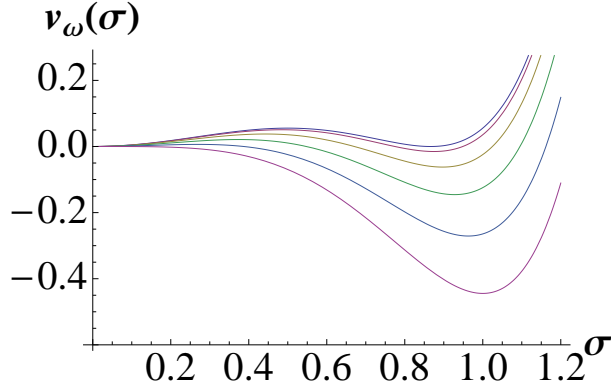


Figure 1. The effective potential V_ω , for different $\omega = 0, 0.2, 0.4, 0.6, 0.8$ and 1.0 . $\omega = 0$ corresponds to a degenerate potential, and increasing ω lowers the non-zero minimum.

For the purposes of this paper we will take the potential to be (see, for instance, Ref. [3])

$$V(\phi) = m^2 \phi^\dagger \phi - \lambda (\phi^\dagger \phi)^2 + \frac{4g}{3} (\phi^\dagger \phi)^3. \quad (1.6)$$

Writing the complex field as $\phi = (\phi_1 + i\phi_2)/\sqrt{2}$, with $\phi_{1,2}$ real-valued, the potential has $O(2)$ symmetry in field space. Let us specialise to the case where the classical potential has degenerate minima for $v_0 = 0$ and $v \neq 0$ (up to global $O(2)$ transformations)

$$m = 1, \quad \lambda = 16/3, \quad g = 16/3 \quad \Rightarrow \quad v = \frac{\sqrt{3}}{2}. \quad (1.7)$$

For $\omega = 0$, the profile function $\sigma_0(r)$ can be easily found using Eq. (1.6) directly. For non-zero ω , by inserting the ansatz as in Eq. (1.4), we should solve for the radial profile in the effective potential¹

$$V_\omega(\sigma) = \frac{m^2 - \omega^2}{2} \sigma^2 - \frac{\lambda}{4} \sigma^4 + \frac{g}{6} \sigma^6. \quad (1.8)$$

Fig. 1 shows the potential for a number of different ω between 0 and 1. We now have

$$v_\pm^2 = \frac{\lambda}{2g} \left(1 + \sqrt{1 - \frac{4}{\lambda^2} (m^2 - \omega^2)} \right), \quad (1.9)$$

and when $\omega > m$, $\phi = 0$ becomes a maximum rather than a minimum. There is then no longer a bump separating v_\pm from $\phi = 0$. Hence for some value $\omega_+ \leq m$, a stable profile function no longer exists. In general there is also a lower limit ω_- following from an additional criterion on the potential, $\min[V_\omega(\sigma)] \leq 0$, that ensures Q-ball solutions are localised. For our case with degenerate vacua, $\omega_- = 0$ [3].

¹We use “effective” to denote the potential when inserting the Q-ball ansatz, and not for the effective quantum potential, for which we use the term “quantum”.

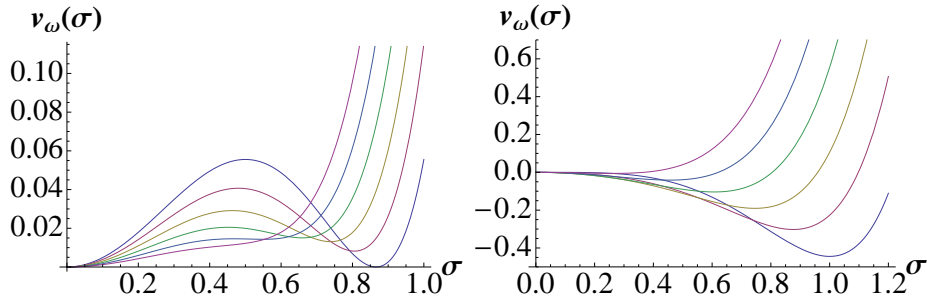


Figure 2. The quantum effective potential $V_{\omega,\text{eff}}$, for different values of G , at $\omega = 0$ (left) and $\omega = 1$ (right). Increasing G lifts the potential at the nonzero minimum away from zero, until it is no longer a minimum.

Further, in order for the Q-ball to be stable to small perturbations, the profile function must be a (local) minimum in field configuration space,

$$\frac{d^2 S_\omega}{d\omega^2} \geq 0, \quad S_\omega = \int d^3x \left[\frac{1}{2} (\nabla\sigma_\omega)^2 + V_\omega(\sigma_\omega) \right]. \quad (1.10)$$

This concludes our brief review of classical Q-balls. An extensive literature on the subject, including many models, can be found in Ref. [4] and references therein.

1.1 Quantum decay: prelude

In Ref. [3], a detailed study of quantum stability was carried out for the potential given in Eq. (1.6) (as well as others), in a varying number of spatial dimensions. After finding the profile functions numerically, two quantum instabilities were considered in addition to the classical stability criterion: the possible decay of a Q-ball into a set of smaller Q-balls (with smaller Q or a set of positive and negative Q-balls adding up to the original Q); or to a set of charged, but particle-like excitations of the field.

If the Q-ball is classically stable, decaying in this way is a tunnelling event, whereby the original profile changes into a different field configuration with particles or several Q-balls. At least in a purely quantum environment (where transitions are not mediated by thermal fluctuations) the transition rate is typically extremely suppressed. Therefore, although unstable to decay in principle, in general the Q-ball is likely to be effectively stable on the timescale of the system, m^{-1} .

In the present work we seek to build upon the results of Ref. [3], by considering the effect of fluctuations in changing the quantum potential in which the Q-ball evolves. Taking the Q-ball to be the mean field (one-point correlator) of the quantum field – evolving in the background of quantum fluctuations – the potential is modified substantially. This will alter the profile function $\sigma_\omega(r)$ for a given ω , and hence change the range of ω within which the criteria for stability are fulfilled.

We will perform fully real-time simulations of Q-balls and fluctuations in the “inhomogeneous Hartree” approximation (see for instance Refs. [6, 7]). This will allow us to capture the leading order effects in a quantum loop expansion, taking into account the

inhomogeneity and time-dependence of the system. Such an approach has previously been successful when applied to topological solitons [8–10].

For such solitons, where the stability is guaranteed by topology and the solution is time-independent, one may do a complete Monte Carlo study as in Ref. [5]. This approach completely bypasses any notion of a classical solution, which is not possible for a time-dependent system such as a Q-ball.

1.2 Quantum decay: homogeneous Hartree approximation

Before we embark on the technical description of this method, we will illustrate the mechanism of instability by first considering what happens to the potential in the “homogeneous Hartree” approximation. This amounts to keeping the equations of motion for the mean field and quantum two-point functions, and throwing away all higher order correlations. In our case, we have the connected equal time propagators

$$G_1 = \langle \phi_1^2 \rangle - \langle \phi_1 \rangle^2, \quad G_2 = \langle \phi_2^2 \rangle - \langle \phi_2 \rangle^2 \quad \text{and} \quad K = \langle \phi_1 \phi_2 \rangle - \langle \phi_1 \rangle \langle \phi_2 \rangle = \langle \phi_2 \phi_1 \rangle - \langle \phi_2 \rangle \langle \phi_1 \rangle. \quad (1.11)$$

In addition, $\Phi_{1,2}$ are the one-point functions of $\phi_{1,2}$. We will derive the equations of motion in Section 2 – specifically, Eqs. (2.6) and (2.9) – but for illustration and to motivate the approach taken in this paper we will make use of them here. For the purposes of this section only, we make the simplistic assumption that $G_1 = G_2 = G$ and $K = 0$, and that they are space and time independent. For the quantum effective potential, this yields²

$$V_{\omega,\text{eff}}(\sigma) = \frac{m^2 - \omega^2 - 4\lambda G + 24gG^2}{2}\sigma^2 - \frac{(\lambda - 12gG)}{4}\sigma^4 + \frac{g}{6}\sigma^6. \quad (1.12)$$

In Fig. 2 we show the quantum effective potential for different values of G for $\omega = 0$ (left hand plot) and $\omega = 1$ (right hand plot). We see that the main effect of including G is that it lifts and eventually removes the non-zero minimum. It is clear that when this minimum is gone, there can be no more stable Q-balls. When $\omega = 1$, the non-zero minimum is the only one until for $G > \frac{1}{6}$, the zero minimum becomes the only one.

The criteria for there to be two minima are that the zero-minimum v_0 should have positive curvature. With our parameters, given in Eq. (1.7), this means

$$\left(\frac{d^2 V_{\omega,\text{eff}}(\sigma)}{d\sigma^2} \right)_{\sigma=0} = (1 - \omega^2) - \frac{64}{3}G + 128G^2 > 0, \quad (1.13)$$

and the non-zero minimum v should exist (it always has positive curvature). Existence of this second minimum is when

$$v^2 = \frac{2 - 24G + \sqrt{1 - 32G + 192G^2 + 3\omega^2}}{4} \quad (1.14)$$

is real and positive. When $1 - 32G + 192G^2 + 3\omega^2 < 0$, the non-zero minimum coalesces with the intermediate maximum that separates v_0 and v . And when $v^2 < 0$, the intermediate maximum coalesces with the minimum v_0 at zero. Hence our second criterion is

$$(1 + 3\omega^2) - 32G + 192G^2 > 0. \quad (1.15)$$

²Compare with Eqs. (2.25) and (2.26), which give the full quantum effective potential without these additional simplifying assumptions.

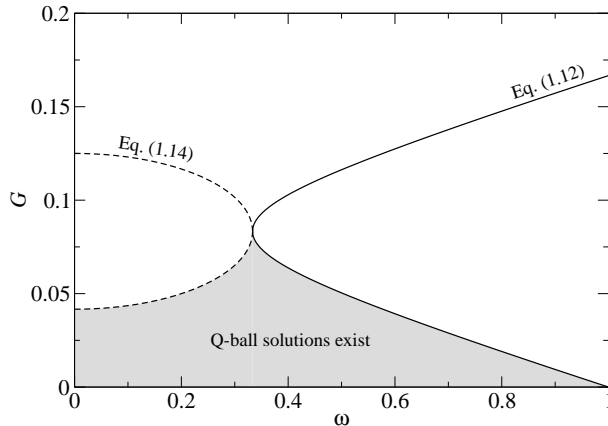


Figure 3. Regions of two, one and no minima in the quantum effective potential. In order for the quantum potential to have two minima, (ω, G) have to be in the bottom left region, below all the curves. In particular, at $G = 0$, $\omega < 1$.

We show in Fig. 3 how these criteria split up the ω/G -plane into a Q-ball region (below the curves), and a single minimum region (the rest). Having G and ω below the curves is a necessary criterion for the existence of Q-balls; but it is not sufficient, since then a proper profile solution has to be found which is stable, further restricting the parameter space. We see that in the classical $G = 0$ limit, Q-balls are stable until some large ω close to $m = 1$. But in the quantum case when G is non-zero, an additional instability region opens up at low ω . This is similar to the emergence of a non-zero ω_- , but to distinguish it from a classical ω_- , we will denote it ω_{limit} .

This qualitative argument also suggests that if the correlator G becomes very large, stability is lost, for this particular set of renormalised parameters in the potential. Different values of the parameters of the potential will lead to modified bounds, but the picture remains the same. Also, when stability is lost in the low- ω region, it is the large-field value minimum that disappears, whereas the classical instability is the high- ω region, when the zero-field minimum becomes a maximum instead of a minimum. The latter instability also happens in the quantum case, but (potentially, depending on G) at smaller or larger values of ω .

1.3 This paper

The effective quantum potential as written in Eq. (1.12) is unsatisfactory in a number of ways. First of all, the correlator K is nonzero in general, and $G_{1,2}$ and K are all time-dependent, since they evolve in the background of a time-dependent mean field. In addition, they are all space-dependent, just like the mean field. They are approximately spherically symmetric, although we will not impose that explicitly here. Also, $G_{1,2}$ are divergent quantities, and we must renormalise the equations of motion appropriately. Although the ϕ^6 interactions formally make the theory non-renormalisable, at the level of the Hartree approximation, this can be done.

We end up solving a set of coupled differential equations for the mean fields $\Phi_{1,2}(\mathbf{x}, t)$ and the corresponding correlators $G_{1,2}(\mathbf{x}, \mathbf{y}, t, t')$. In addition, we have the cross-correlators

$$K(\mathbf{x}, \mathbf{y}, t, t') = \langle \phi_1(\mathbf{x}, t) \phi_2(\mathbf{y}, t') \rangle - \langle \phi_1(\mathbf{x}, t) \rangle \langle \phi_2(\mathbf{y}, t') \rangle \quad (1.16a)$$

$$\text{and } \bar{K}(\mathbf{x}, \mathbf{y}, t, t') = \langle \phi_2(\mathbf{y}, t') \phi_1(\mathbf{x}, t) \rangle - \langle \phi_2(\mathbf{y}, t') \rangle \langle \phi_1(\mathbf{x}, t) \rangle. \quad (1.16b)$$

Note that K and \bar{K} coincide at equal time and space, but not in general. In fact, we will instead make use of the method of Refs. [6, 7], where each quantum mode of the fluctuations is solved for in the background of the mean field. For reasons of computer time, we will further replace that by a classical-statistical ensemble computation of the mode correlators $G_{1,2}$ and K, \bar{K} [9].

In Section 2, we will introduce the inhomogeneous Hartree approximation and the ensemble method and renormalisation of the equations of motion. Readers with less interest in the technicalities may wish to skip to Section 3 where we show our results for the stability region as a function of ω (note that G is then no longer a free parameter, but follows from the dynamics). We conclude in Section 4.

2 The inhomogeneous Hartree approximation

As mentioned, we consider a self-interacting complex scalar field $\phi = (\phi_1 + i\phi_2)/\sqrt{2}$, with classical action

$$S = - \int d^3x dt \left[(\partial_\mu \phi)^\dagger (\partial^\mu \phi) + m^2 \phi^\dagger \phi + \lambda (\phi^\dagger \phi)^2 + \frac{4g}{3} (\phi^\dagger \phi)^3 \right]. \quad (2.1)$$

We find it advantageous to recast the equations in terms of the two real-valued fields ϕ_1 and ϕ_2 , and define the quantum mechanical one-point functions

$$\langle \phi_1 \rangle = \Phi_1, \quad \langle \phi_2 \rangle = \Phi_2, \quad (2.2)$$

as well as a matrix of connected two-point functions

$$\mathcal{G} = \begin{pmatrix} G_1(x, y) & K(x, y) \\ \bar{K}(x, y) & G_2(x, y) \end{pmatrix}, \quad (2.3)$$

where

$$G_1(x, y) = \langle \phi_1(x) \phi_1(y) \rangle - \langle \phi_1(x) \rangle \langle \phi_1(y) \rangle, \quad (2.4a)$$

$$G_2(x, y) = \langle \phi_2(x) \phi_2(y) \rangle - \langle \phi_2(x) \rangle \langle \phi_2(y) \rangle, \quad (2.4b)$$

$$K(x, y) = \langle \phi_1(x) \phi_2(y) \rangle - \langle \phi_1(x) \rangle \langle \phi_2(y) \rangle \quad (2.4c)$$

$$\text{and } \bar{K}(x, y) = \langle \phi_2(x) \phi_1(y) \rangle - \langle \phi_2(x) \rangle \langle \phi_1(y) \rangle. \quad (2.4d)$$

We note that

$$G_1(x, y) = G_1(y, x), \quad G_2(x, y) = G_2(y, x), \quad K(y, x) = \bar{K}(x, y) \Rightarrow K(x, x) = \bar{K}(x, x). \quad (2.5)$$

We will denote $G_{1,2}(x, x) = G_{1,2}$, and similarly $K(x, x) = K = \bar{K}$. The Heisenberg equations of motion read

$$[\partial_t^2 - \partial_x^2 + m^2 - \lambda(\phi_1^2 + \phi_2^2) + g(\phi_1^2 + \phi_2^2)^2] \phi_1 = 0 \quad (2.6a)$$

$$\text{and } [\partial_t^2 - \partial_x^2 + m^2 - \lambda(\phi_1^2 + \phi_2^2) + g(\phi_1^2 + \phi_2^2)^2] \phi_2 = 0. \quad (2.6b)$$

We then take expectation values of Eq. (2.6), to get the equation of motion for the mean field Φ_1 (and by symmetry for Φ_2), keeping only one- and two-point functions:

$$[\partial_\mu \partial^\mu - M_{11}^2(x)] \Phi_1(x) - M_{12}^2(x) \Phi_2(x) = 0 \quad (2.7a)$$

$$\text{and } [\partial_\mu \partial^\mu - M_{22}^2(x)] \Phi_2(x) - M_{21}^2(x) \Phi_1(x) = 0 \quad (2.7b)$$

with

$$\begin{aligned} M_{11}^2 &= m^2 - \lambda(\Phi_1^2 + \Phi_2^2 + 3G_1 + G_2) + g(\Phi_1^4 + \Phi_2^4 + 2\Phi_1^2\Phi_2^2) \\ &\quad + g(15G_1^2 + 3G_2^2 + 10G_1\Phi_1^2 + 6G_2\Phi_2^2 + 6G_1\Phi_2^2 + 2G_2\Phi_1^2 + 6G_1G_2) \\ &\quad + 12gK(K + \Phi_1\Phi_2) \end{aligned} \quad (2.8a)$$

$$\text{and } M_{12}^2 = -2\lambda K + 4gK(\Phi_2^2 + 3G_1 + 3G_2); \quad (2.8b)$$

M_{22}^2 and M_{21}^2 are obtained by interchanging the field subscripts 1 and 2 in the expressions for M_{11}^2 and M_{12}^2 respectively. We can also multiply Eq. (2.6) by $\phi^*(y)$ from the right and take the expectation value, again keeping only one- and two-point functions, to get

$$[\partial^2 - \tilde{M}_{11}^2(x)] G_1(x, y) - \tilde{M}_{12}^2(x) \bar{K}(x, y) = 0, \quad (2.9a)$$

$$[\partial^2 - \tilde{M}_{22}^2(x)] G_2(x, y) - \tilde{M}_{21}^2(x) K(x, y) = 0, \quad (2.9b)$$

$$[\partial^2 - \tilde{M}_{11}^2(x)] K(x, y) - \tilde{M}_{12}^2(x) G_2(x, y) = 0, \quad (2.9c)$$

$$[\partial^2 - \tilde{M}_{22}^2(x)] \bar{K}(x, y) - \tilde{M}_{21}^2(x) G_1(x, y) = 0, \quad (2.9d)$$

with

$$\begin{aligned} \tilde{M}_{11}^2 &= m^2 - \lambda(3\Phi_1^2 + \Phi_2^2 + 3G_1 + G_2) + g(5\Phi_1^4 + \Phi_2^4 + 6\Phi_1^2\Phi_2^2) \\ &\quad + g(15G_1^2 + 3G_2^2 + 30G_1\Phi_1^2 + 6G_2\Phi_2^2 + 6G_1\Phi_2^2 + 6G_2\Phi_1^2 + 6G_1G_2) \\ &\quad + 12gK(K + 2\Phi_1\Phi_2), \end{aligned} \quad (2.10a)$$

$$\begin{aligned} \text{and } \tilde{M}_{12}^2 &= -2\lambda(K + \Phi_1\Phi_2) \\ &\quad + 4g(\Phi_1^3\Phi_2 + \Phi_2^3\Phi_1 + 3\Phi_1\Phi_2(G_1 + G_2)) \\ &\quad + 12gK(\Phi_1^2 + \Phi_2^2 + G_1 + G_2); \end{aligned} \quad (2.10b)$$

\tilde{M}_{22}^2 and \tilde{M}_{21}^2 being obtained as before. Truncating the Schwinger-Dyson hierarchy in this way at the level of one- and two-point functions constitutes the Hartree approximation. It is the leading order truncation of a 2PI loop expansion (see for instance Ref. [11]).

The equations of motion are discretised in a straightforward way on a three-dimensional lattice. The differential equations are solved using a simple leapfrog algorithm in time.

In the homogeneous Hartree case, there is translational invariance $\Phi_1(x) = \Phi_1(t)$, $\Phi_2(x) = \Phi_2(t)$, and we could write

$$G_1(x, y) = G_1(x - y), G_2(x, y) = G_2(x - y), K(x, y) = K(x - y) \text{ and } \bar{K}(x, y) = \bar{K}(x - y). \quad (2.11)$$

The resulting equations can be solved numerically in a very efficient manner [12]. In the limit of the time dependence also being trivial, the system reduces to a simple gap equation. However, since the Q-ball is inhomogeneous and time-dependent, these simplifications are not possible, and we will have to solve for the whole inhomogeneous Hartree approximation [6, 7]. This means that on a d -dimensional lattice with N sites in each direction, the problem scales as N^{2d} . This is numerically possible in one spatial dimension, but at present not reliably in three.

2.1 Ensemble bosons

Rather than solving the evolution in terms of the one- and two-point functions, we will take advantage of the fact that a Gaussian system (free or truncated at the Hartree level) may be represented in terms of mode functions. We write (for either of the two fields $j = 1, 2$)

$$\phi_j(\mathbf{x}, t) = \Phi_j(\mathbf{x}, t) + \int \frac{d^3k}{(2\pi)^3} \left[a_{\mathbf{k}} f_{\mathbf{k}}^j(\mathbf{x}, t) + a_{\mathbf{k}}^\dagger f_{\mathbf{k}}^{j*}(\mathbf{x}, t) \right]. \quad (2.12)$$

The operators $a_{\mathbf{k}}$ are time-independent by virtue of the Gaussian approximation, and they are the standard creation-annihilation operators obeying the relations

$$[a_{\mathbf{k}}, a_{\mathbf{l}}^\dagger] = \delta_{\mathbf{k}, \mathbf{l}} \quad \text{and} \quad [a_{\mathbf{k}}, a_{\mathbf{l}}] = [a_{\mathbf{k}}^\dagger, a_{\mathbf{l}}^\dagger] = 0. \quad (2.13)$$

In particular, the occupation number $n_{\mathbf{k}}$ in some state is given by

$$\langle a_{\mathbf{k}}^\dagger a_{\mathbf{k}} \rangle = n_{\mathbf{k}}. \quad (2.14)$$

Since the $a_{\mathbf{k}}$ are time independent, the numbers $n_{\mathbf{k}}$ encode all necessary information about the initial state. The mode functions $f_{\mathbf{k}}^j(\mathbf{x}, t)$ are (complex-valued) solutions of the two-point function equations of motion given in Eq. (2.9)

$$\left[\partial^2 - \tilde{M}_{11}^2(x) \right] f_{\mathbf{k}}^1(x) - \tilde{M}_{12}^2 f_{\mathbf{k}}^2(x) = 0 \quad (2.15a)$$

$$\text{and } \left[\partial^2 - \tilde{M}_{22}^2(x) \right] f_{\mathbf{k}}^2(x) - \tilde{M}_{21}^2 f_{\mathbf{k}}^1(x) = 0. \quad (2.15b)$$

In the vacuum $\Phi_1 = \Phi_2 = 0$, the solutions are plane waves,

$$f_{\mathbf{k}}^j(\mathbf{x}, t) = \frac{1}{\sqrt{2\omega_{\mathbf{k}}}} e^{i\mathbf{k}\mathbf{x} - i\omega_{\mathbf{k}}t}, \quad \omega_{\mathbf{k}}^2 = k^2 + m^2, \quad (2.16)$$

but in a general background $\Phi_i(x)$ this is no longer the case. We will nevertheless use Eq. (2.16) as our initial condition.

Numerically, discretising space on a N^3 lattice, there are N^3 mode functions for each of the two fields in this model, and so the effort of solving for them all still scales as N^6 .

Fortunately, an alternative exists [9]. Instead of solving at the level of $f_{\mathbf{k}}^j(x)$, and then computing

$$G_j(x, x) = \int \frac{d^3 k}{(2\pi)^3} (2n_{\mathbf{k}} + 1) |f_{\mathbf{k}}^j|^2(x), \quad (2.17)$$

one may generate a set of random numbers $\{c_{\mathbf{k}}\}$ and $\{d_{\mathbf{k}}\}$, so that for each \mathbf{k} ,

$$\langle c_{\mathbf{k}}^* c_{\mathbf{k}} \rangle_{\text{ensemble}} = \langle d_{\mathbf{k}}^* d_{\mathbf{k}} \rangle_{\text{ensemble}} = n_{\mathbf{k}}, \quad (2.18)$$

and then construct an ensemble of realisations ($i = 1, \dots, M$)

$$\varphi_1^i(\mathbf{x}, 0) = \int \frac{d^3 k}{(2\pi)^3} [c_{\mathbf{k}}^i f_{\mathbf{k}}^1(\mathbf{x}, 0) + (c_{\mathbf{k}}^i)^* f_{\mathbf{k}}^{1*}(\mathbf{x}, 0)], \quad (2.19a)$$

$$\varphi_2^i(\mathbf{x}, 0) = \int \frac{d^3 k}{(2\pi)^3} [d_{\mathbf{k}}^i f_{\mathbf{k}}^2(\mathbf{x}, 0) + (d_{\mathbf{k}}^i)^* f_{\mathbf{k}}^{2*}(\mathbf{x}, 0)], \quad (2.19b)$$

with $f_{\mathbf{k}}^j(\mathbf{x}, 0)$ given by Eq. (2.16) at the initial time. Then one evolves the M random realisations $\varphi_{1,2}^i$ using Eq. (2.15) while simultaneously evolving $\Phi_{1,2}(x)$. At every time step one computes

$$G_1(x, x) = \langle \varphi_1(x)^2 \rangle_{\text{ensemble}} - \langle \varphi_1(x) \rangle_{\text{ensemble}}^2 \quad (2.20a)$$

$$G_2(x, x) = \langle \varphi_2(x)^2 \rangle_{\text{ensemble}} - \langle \varphi_2(x) \rangle_{\text{ensemble}}^2 \quad (2.20b)$$

$$K(x, x) = \langle \varphi_1(x) \varphi_2(x) \rangle_{\text{ensemble}} - \langle \varphi_1(x) \rangle_{\text{ensemble}} \langle \varphi_2(x) \rangle_{\text{ensemble}} \quad (2.20c)$$

recalling that $K(x, x) = \bar{K}(x, x)$. We should also have $\langle \varphi_{1,2}(x) \rangle_{\text{ensemble}} \approx 0$. Although not exact (as computing all the mode functions would be), for M large enough a very good statistical approximation results. As long as $M < N^3$, we have gained in computer efficiency; we will typically be using $N = 64$ and $M = 16384$, for a speed-up of a factor of 16.

2.2 Global and local observables

As our observables for tracking the evolution of the system, we will in addition to the mean fields ($\Phi_{1,2}$) and correlators ($G_{1,2}, K$) themselves consider the charge in the mean field

$$Q_{\Phi}(t) = \int d^3 x j_{\Phi}^0(\mathbf{x}, t) = \int d^3 x i [(\partial_t \Phi_2(\mathbf{x}, t)) \Phi_1(\mathbf{x}, t) - (\partial_t \Phi_1(\mathbf{x}, t)) \Phi_2(\mathbf{x}, t)]; \quad (2.21)$$

and in the modes

$$Q_G(t) = \int d^3 x j_G^0(\mathbf{x}, t) = \int d^3 x \langle i [(\partial_t \varphi_2(\mathbf{x}, t)) \varphi_1(\mathbf{x}, t) - (\partial_t \varphi_1(\mathbf{x}, t)) \varphi_2(\mathbf{x}, t)] \rangle_{\text{ensemble}}; \quad (2.22)$$

and their sum, which should be conserved. In a similar manner, we also consider the energy in the mean field

$$E_{\Phi} = \int d^3 x \rho_{\Phi} = \int d^3 x \left[\frac{1}{2} (\partial_t \Phi_1)^2 + \frac{1}{2} (\partial_t \Phi_2)^2 + \frac{1}{2} (\partial_x \Phi_1)^2 + \frac{1}{2} (\partial_x \Phi_2)^2 + V_{\text{eff}}(\Phi_1, \Phi_2, G_1, G_2, K) \right]; \quad (2.23)$$

and in the modes

$$E_G = \int d^3x \rho_G = \int d^3x \left\langle \left[\frac{1}{2}(\partial_t \varphi_1)^2 + \frac{1}{2}(\partial_t \varphi_2)^2 + \frac{1}{2}(\partial_x \varphi_1)^2 + \frac{1}{2}(\partial_x \varphi_2)^2 + V_{\text{eff}}(G_1, G_2, K) \right] \right\rangle_{\text{ensemble}}; \quad (2.24)$$

the sum of which should again be conserved. We have split the quantum effective potential into two parts; one with mean field and mixed terms,

$$\begin{aligned} V_{\text{eff}}(\Phi_1, \Phi_2, G_1, G_2, K) = & \frac{m^2}{2}(\Phi_1^2 + \Phi_2^2) - \frac{\lambda}{4}(\Phi_1^4 + \Phi_2^4 + 2\Phi_1^2\Phi_2^2 + \\ & 2G_1\Phi_2^2 + 2G_2\Phi_1^2 + 8K\Phi_1\Phi_2 + 6G_1\Phi_1^2 + 6G_2\Phi_2^2) + \\ & \frac{g}{6}(\Phi_1^6 + \Phi_2^6 + 3\Phi_1^2\Phi_2^4 + 3\Phi_2^2\Phi_1^4 + 15\Phi_1^4G_1 + 15\Phi_2^4G_2 + \\ & 18\Phi_1^2\Phi_2^2(G_1 + G_2) + 3\Phi_2^4G_1 + 3\Phi_1^4G_2 + 45\Phi_1^2G_1^2 + 45\Phi_2^2G_2^2 + \\ & 9\Phi_1^2G_2^2 + 9\Phi_2^2G_1^2 + 24\Phi_1\Phi_2K(\Phi_1^2 + \Phi_2^2) + \\ & 72\Phi_1\Phi_2K(G_1 + G_2) + 18(\Phi_1^2 + \Phi_2^2)(G_1G_2 + 2K^2)), \end{aligned} \quad (2.25)$$

and one with only $G_{1,2}$ and K contributions,

$$\begin{aligned} V_{\text{eff}}(G_1, G_2, K) = & \frac{m^2}{2}(G_1 + G_2) - \frac{\lambda}{4}(3G_1^2 + 3G_2^2 + 2G_1G_2 + 4K^2) + \\ & \frac{g}{6}((9G_2G_1 + 36K^2)(G_1 + G_2) + 15G_1^3 + 15G_2^3). \end{aligned} \quad (2.26)$$

The sum of the two is obtained by simply taking the expectation value of the potential and keeping only one- and two-point functions. Note that we choose to assign the interaction energy to the mean field component.

2.3 Renormalisation

The correlators G_1 and G_2 are quadratically and logarithmically divergent, so that in the vacuum with a particular mass $M^2 = m^2 + \delta M^2(\Phi_1, \Phi_2, G_1, G_2, K)$, we have

$$\begin{aligned} G_{1,2} = & \int \frac{d^3k}{(2\pi)^3} \frac{1}{2\sqrt{k^2 + m^2 + \delta M_{1,2}^2}} \\ = & \int \frac{d^3k}{(2\pi)^3} \frac{1}{2\sqrt{k^2 + m^2}} - \frac{\delta M_{1,2}^2}{2} \int \frac{d^3k}{(2\pi)^3} \frac{1}{2(k^2 + m^2)^{3/2}} + \text{finite}. \end{aligned} \quad (2.27)$$

Defining the integrands

$$A \equiv \int^\Lambda \frac{d^3k}{(2\pi)^3} \frac{1}{2\sqrt{k^2 + m^2}} \quad \text{and} \quad B \equiv \int^\Lambda \frac{d^3k}{(2\pi)^3} \frac{1}{2(k^2 + m^2)^{3/2}}, \quad (2.28)$$

the most straightforward way to renormalise is to subtract the non-field dependent part A (computed as a mode sum on the finite lattice) from the correlator everywhere in the

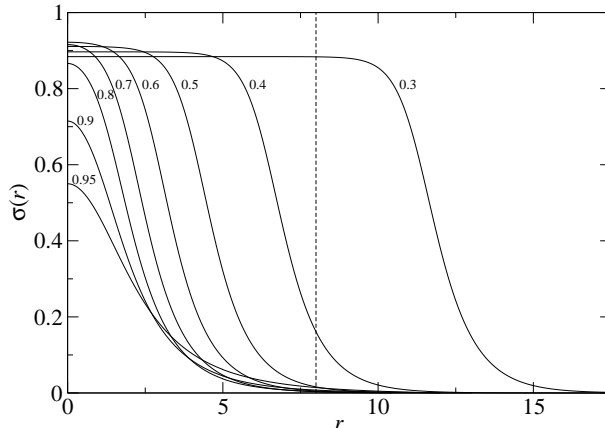


Figure 4. The radial profiles of classical Q-balls for different values of ω . Small ω give spatially large Q-balls. The vertical dashed line at $r = 8$ indicates the radius of the ‘box’ used to compare the charge and energy remaining within the Q-ball.

equations of motion. This amounts to a mass and a coupling renormalisation, since it is equivalent to introducing the counterterms

$$m^2 \rightarrow m^2 + \delta m_A^2 = m^2 - 4\lambda A + 24gA^2, \quad (2.29a)$$

$$\lambda \rightarrow \lambda + \delta\lambda_A = \lambda - 12gA. \quad (2.29b)$$

This approach gets rid of all quadratic divergences, leaving some logarithmic divergences. For the parameters we will be using, $\lambda + \delta\lambda \simeq -0.133$, which means that without renormalisation, there would likely be no stable Q-balls at all. This approach to renormalisation is very similar to the one used for instance in Ref. [13], and is easily generalised to in principle non-renormalisable potentials. It is not, however a completely rigorous 2PI renormalisation scheme (as for instance in Ref. [14] for renormalisable ϕ^4 theory). For our purpose, where we do not go to the strict continuum limit, the present renormalisation scheme will be sufficient.

3 Results

We first find the classical Q-ball profile functions through a standard shooting method, very similar to Ref. [4]. These profiles are displayed in Fig. 4, for a number of different values of ω . Table 1 shows the total charge Q for a number of values of ω .

ω	0.3	0.4	0.5	0.6	0.7	0.8	0.9	0.95
Q	1438.5	368.5	132.5	59.4	31.3	19.1	14.4	15.0

Table 1. Total charge for Q-balls with different ω .

We see that small ω corresponds to large Q , and to large radial size; in this limit the thin wall approximation can be applied [1]. In particular, for the size of lattices we are

able to treat numerically with the inhomogeneous Hartree implementation at a sufficiently large mode ensemble, we were unable to go below $\omega = 0.3$. This will not influence our findings. At the other end, large ω corresponds to small Q and in this limit a Gaussian ansatz describes a classical Q-ball well [15].

As a check of our shooting, we evolve the initial profiles using classical dynamics, for comparison with the Hartree evolution. Indeed, charge and energy are well conserved at all times, and the Q-balls are classically stable for all $\omega \leq 0.99$, at least on the timescale of our simulations. In particular, we see no sign of the classical instability reported in Ref. [3] for $\omega > 0.92$. We also checked that the results (quantum, and where applicable, classical) were stable under variation in the number of ensemble members M , lattice size and spacing and time step; the results presented here were obtained with a lattice spacing of $a = 0.5/m$.

We define a spherical ‘box’ around the Q-ball, for which we evaluate the energy and charge ‘inside’ the Q-ball, as opposed to outside; the centre of the box tracks the barycentre of the charge in the system. Outside energy and charge is then taken to have ‘decayed’ off the Q-ball. This applies to both modes and mean field separately and combined. The box has a radius of 8 in inverse mass units. Further outside, at a radius > 12 in inverse mass units, we have a region with damping, to minimise the amount of released energy and charge that can reach the boundary, go around the lattice and affect the Q-ball. This is meant to emulate the mechanism by which a Q-ball would decay into the surrounding vacuum. In a simulation of many Q-balls created, say, during a phase transition, the situation would be different. But for our purposes here, the Q-ball is alone. We checked that the exact choice of damping rate is not important, although it must be non-zero.

We start with a stable example, taking $\omega = 0.8$. Fig. 5 shows the charge inside the ‘box’ in the complete system (red; solid), in the mean field (green; dashed) and in the modes (blue; dot-dash). The black dashed line is the classical simulation. We see that the Q-ball is stable also in the quantum case, and that the charge has the same value as for the classical case. On the face of it, this suggests that quantum effects are very small. But we see that in the quantum case the charge is exchanged almost completely between the mean field and modes, an effect which simply is absent from the classical simulation. And so although the quantum system is very different, charge conservation is still realised as a quantum symmetry. There is some statistical noise coming from the mode averaging, even at $M = 16384$ (it was unacceptably severe at $M = 2048$), so that the charge within the Q-ball is not quite as smooth as the classical simulation. Still, we find the agreement compelling.

In Fig. 6, we show the case of $\omega = 0.7$, again inside the ‘box’ and again the total (red; solid), mean field (green; dashed), mode (blue; dot-dash) and classical (black) charge. The Q-ball collapses around time 8 (in inverse mass units), and after time 14 the system becomes very noisy. We see that charge completely vacates the central box volume. This is a true effect, and can be seen from considering the charge density, as shown in the snapshots in Fig. 7. They correspond to times $t = 0, 8$ and 16 in the evolution and show positive (blue) and negative (red) charge density in space.

We have checked that a similar collapse signature appears in the energy inside the

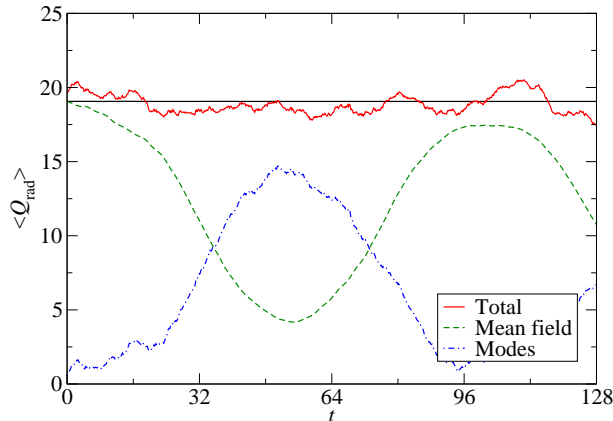


Figure 5. The total (red; solid), mean field (green; dashed) and mode (blue; dot-dash) charge, compared to a purely classical run (black) from the same initial profile. Here $\omega = 0.8$, and the Q-ball is stable both in the quantum and classical systems.

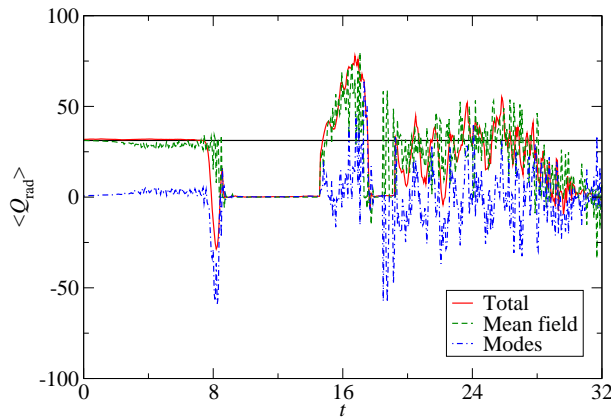


Figure 6. The total (red; solid), mean field (green; dashed) and mode (blue; dot-dash) charge, compared to a purely classical run (black) from the same initial profile. Here $\omega = 0.7$, and the Q-ball is unstable in the quantum system. The decay happens at around $t = 8$.

box. Clearly, the Q-ball is unstable in the quantum case, but not in the classical case. In addition, we notice that in contrast to the classical case, where instability appears above some large ω , we now have instability below a certain limit ω_{limit} . As one gets closer to this limiting value from below, the lifetime gets longer and suddenly becomes much longer than the duration of our simulations. Fig. 8 shows these lifetimes, and we identify the limiting value as lying in the range

$$0.78 < \omega_{\text{limit}} < 0.79. \quad (3.1)$$

We finish by showing the charge evolution for $\omega = 0.95$, which based on the criteria of Ref. [3] is expected to be classically unstable, and quantum unstable to fission. Our approximation does not include fission, but nor does it explicitly impose spherical symmetry

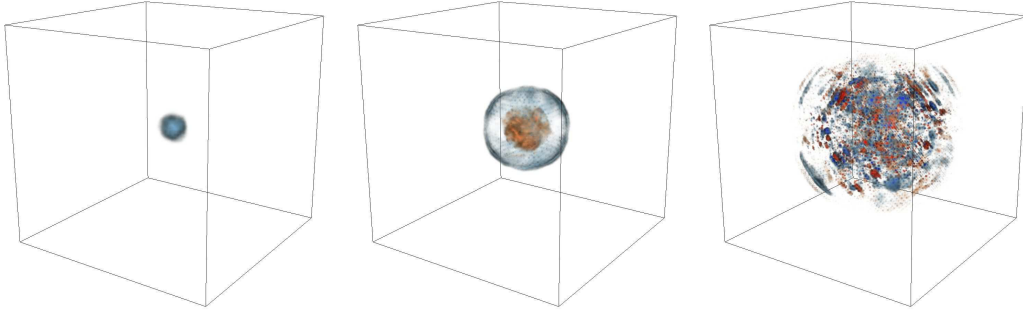


Figure 7. Snapshots of the charge density for the $\omega = 0.7$ run shown in Fig. 6 at times $t = 0, 8$ and 16 in inverse mass units. Blue is positive charge density, red is negative.

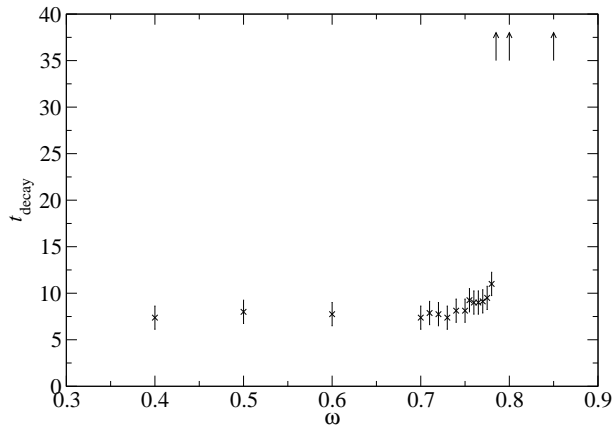


Figure 8. The lifetime as a function of ω . Simulations at and above $\omega = 0.785$ do not decay before $t = 128$, the maximum duration of our simulations.

(the initial condition is spherically symmetric, but implemented on a cubic lattice), so collapse into non-spherically symmetric collections of smaller objects is in principle possible. We see in Fig. 9 that the Q-ball is both classically and quantum mechanically stable on the time scales considered here. Classical stability is of course lost for $\omega \geq 1$, but even at $\omega = 0.99$ we found classical stability in the real-time numerical evolution.

4 Conclusion

Inspired by the comprehensive work of Ref. [3], we have implemented the inhomogeneous Hartree approximation to quantum dynamics for Q-balls in a particular classical potential, with a particular set of parameters. The classical potential is of the “degenerate minima” type, where there are two classical minima, separated by a maximum. Based on general criteria, Q-balls are expected to be unstable to quantum decay into smaller objects for $\omega > 0.82$, and otherwise completely stable. They are classically unstable for even larger

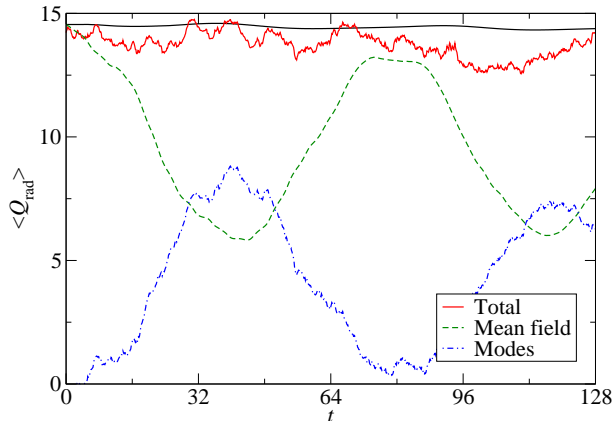


Figure 9. The total (red; solid), mean field (green; dashed) and mode (blue; dot-dash) charge, compared to a purely classical run (black) from the same initial profile. $\omega = 0.95$, and the Q-ball is stable also in the quantum system. The small oscillation in the classical charge arises from the damping at large radii.

$\omega > 0.92$, as the minimum at $\phi = 0$ becomes too shallow to support a Q-ball, and effectively disappears.

Our findings represent interesting complementary information to this result. To leading order in a 2PI loop expansion, we found that quantum corrections to the effective potential in which the mean field Q-ball lives change the picture completely. There is now a limiting ω around 0.78-0.79 *below* which Q-balls are unstable to collapse. Not through tunnelling or decay as for the quantum instability discussed in Ref. [3], but classical-like collapse as the non-zero minimum becomes shallow and – perhaps – effectively disappears. Above this limiting frequency, the Q-balls are stable at least up to the maximum $\omega = 0.99$ tested.

We are not able to go beyond $\omega = 1$, since there are no classical initial profiles there. In addition, for numerical reasons we are also unable to go below $\omega = 0.3$ to see whether stability reappears. As far as we have been able to go, there is no sign of this, and our qualitative analysis in Section 1.1 suggests the same.

The main caveat to these conclusions is that the chosen potential has quite large bare parameters, and considering the Hartree approximation as a coupling expansion it is possible that this truncation is not reliable. In a sense, the exact quantum effective potential would include the precise local potential form, quantum tunnelling and non-perturbative decay. For an unstable mean field configuration, it may even have a physically significant imaginary part, signalling this instability. Clearly, the Hartree approximation does not include tunnelling, but is here assumed to give the dominant contribution to the local shape of the potential near the minima, ultimately changing minima and maxima into maxima and minima. One may fear that this is a crude approximation. On the other hand, the Hartree approximation is an infinite resummation of perturbative diagrams. Order counting in a 2PI expansion also involves the magnitude of the propagator, which is rather small here. Ideally, one would like to go to the next order in this expansion, but

currently 2PI-NLO is not numerically tractable for an inhomogeneous system.

In summary, when studying the quantum stability of Q-balls it is perhaps more important to understand the modification of the mean field potential, than the non-perturbative decay and tunnelling of the classical solutions. This is because tunnelling typically occurs on very long timescales, although estimating the decay rate is very difficult. It is not clear that the classical profile function is the correct starting point for such a tunnelling transition, since the quantum potential is different. Furthermore, when considering the corrected quantum effective potential (in our case in the Hartree approximation), one finds a qualitatively different stability pattern as a function of ω . The non-zero minimum can disappear for large G and Q-ball solutions no longer exist. This happens on a very short timescale of a few tens of inverse mass units (essentially the time it takes for the quantum effective potential to settle in our simulations).

We have argued that an analysis of the instability (as in Section 1.1) gives the correct qualitative understanding of the Q-ball decay, but that quantitative understanding would require large-scale simulations. In particular, we found that at least $M = 16384$ mode realisations are necessary for statistical convergence of the method when $N = 64$, and for instance that $M = 2048$ is insufficient.

Finally, we have shown that the quantum effects are significant in this model, as charge is almost completely transferred between the mean field and the quantum modes. This is despite the general consensus that a Q-ball will essentially behave classically. That assumption needs to be more rigorously tested in future work.

Many classical simulations of Q-ball formation, evolution and interactions have been carried out [16–19]. The present work demonstrates that the dynamics of quantum Q-balls may be very different from that of classical Q-balls, and that it is feasible to simulate quantum Q-ball behaviour. Such Q-ball simulations should therefore be revisited.

For precision computations, it may be relevant to improve on the renormalisation procedure, since in addition to physical modifications of the potential, some effects may remain of using our approximate subtraction scheme. The main result of this is that at finite lattice spacing, matching the renormalised couplings to be equal to the classical ones is not exact, as one would ideally wish. The effective modification of the potential is therefore in small part due to this. This may be remedied order by order in a loop expansion, although the fully resummed counterterm procedure of Ref. [14] may not generalise to non-renormalisable potentials.

The obvious generalisation is to consider other parameter choices and different theories of Q-balls, in addition to the single example presented here. It could also be interesting to do a completely classical-statistical simulation of the system as an approximation to the quantum Q-ball system. This would involve generating an appropriate ensemble of initial conditions to evolve classically and average over. These projects are both underway.

Acknowledgments: The numerical simulations were performed on the Norwegian computer cluster Abel, under the NOTUR project. AT thanks the Villum foundation for support and DJW thanks Mark Hindmarsh and Arttu Rajantie for stimulating discussions. We thank Paul Saffin for useful comments.

References

- [1] S. R. Coleman, Nucl. Phys. B **262** (1985) 263 [Erratum-ibid. B **269** (1986) 744].
- [2] R. Friedberg, T. D. Lee and A. Sirlin, Phys. Rev. D **13** (1976) 2739.
- [3] M. I. Tsumagari, E. J. Copeland and P. M. Saffin, Phys. Rev. D **78** (2008) 065021 [arXiv:0805.3233 [hep-th]].
- [4] M. I. Tsumagari, “The Physics of Q-Balls,” Ph.D. Thesis, University of Nottingham (2009) [arXiv:0910.3845 [hep-th]].
- [5] A. Rajantie and D. J. Weir, Phys. Rev. D **82** (2010) 111502 [arXiv:1006.2410 [hep-lat]].
- [6] M. Salle, J. Smit and J. C. Vink, Phys. Rev. D **64** (2001) 025016 [hep-ph/0012346].
- [7] M. Salle, J. Smit and J. C. Vink, Nucl. Phys. B **625** (2002) 495 [hep-ph/0012362].
- [8] M. Salle, Phys. Rev. D **69** (2004) 025005 [hep-ph/0307080].
- [9] S. Borsanyi and M. Hindmarsh, Phys. Rev. D **77** (2008) 045022 [arXiv:0712.0300 [hep-ph]].
- [10] Y. Bergner and L. M. A. Bettencourt, Phys. Rev. D **69** (2004) 045002 [hep-th/0305190].
- [11] J. Berges, AIP Conf. Proc. **739** (2005) 3 [hep-ph/0409233].
- [12] G. Aarts, G. F. Bonini and C. Wetterich, Phys. Rev. D **63** (2001) 025012 [hep-ph/0007357].
- [13] A. Arrizabalaga, J. Smit and A. Tranberg, Phys. Rev. D **72** (2005) 025014 [hep-ph/0503287].
- [14] G. Fejos, A. Patkos and Zs. Szep, Nucl. Phys. A **803** (2008) 115 [arXiv:0711.2933 [hep-ph]].
- [15] M. Gleiser and J. Thorarinson, Phys. Rev. D **73** (2006) 065008 [hep-th/0505251].
- [16] R. Battye and P. Sutcliffe, Nucl. Phys. B **590** (2000) 329 [hep-th/0003252].
- [17] K. Enqvist, A. Jokinen, T. Multamaki and I. Vilja, Phys. Rev. D **63** (2001) 083501 [hep-ph/0011134].
- [18] T. Multamaki and I. Vilja, Phys. Lett. B **535** (2002) 170 [hep-ph/0203195].
- [19] T. Hiramatsu, M. Kawasaki and F. Takahashi, JCAP **1006** (2010) 008 [arXiv:1003.1779 [hep-ph]].